An extended semiclassical initial value representation approach to IR spectroscopy

Cecilia Lanzi, Chiara Aieta, Michele Ceotto, and Riccardo Conte*

Dipartimento di Chimica, Università degli Studi di Milano,

via Golgi 19, 20133 Milano, Italy

Abstract

Recently - C. Lanzi *et al. J. Chem. Phys.* **160**, 214107 (2024) - we introduced a time averaged approach to infrared (IR) spectroscopy. The pivotal advance in that paper was represented by the possibility to get accurate semiclassical estimates of the IR absorption intensities and associated transition frequencies from a single calculation. However, the method relies on the convergence of Monte Carlo integrations based on the generation of thousands of pairs of semiclassical trajectories. This makes the approach highly accurate but limited to small, few-atom molecules. Here we build on the theoretical grounds of that work to extend the application of the method to larger molecules. The goal is achieved by moving to tailored single-pair trajectory calculations and introducing a partially time-independent approximation to the real part of the coherent state overlap. Upon testing the level of accuracy on small molecules like water, formaldehyde, and methane, we calculate IR spectra for ethanol and glycine. Vibrational intensities and frequencies are found to be fairly accurate, and the method can be straightforwardly applied to larger molecular systems.

*Electronic address: riccardo.conte1@unimi.it

I. INTRODUCTION

IR spectroscopy is an experimental technique commonly employed in chemistry, able to provide information on molecular structure and interactions.[1] Despite being widely employed, experimental IR spectra are often difficult to assign. Theoretical approaches may help to overcome this issue. However, calculation of IR spectra is a hard task due to the necessity to estimate accurately both the frequencies and the intensities associated to quantum mechanical vibrational transitions.

A classical approach to the problem consists in calculating the Fourier transform of the dipole moment autocorrelation function.[2] The resulting spectrum provides a classical estimate of the vibrational frequencies and absorption intensities of the system. If one is interested in frequencies only, then a power spectrum can be computed as the Fourier transform of the velocity autocorrelation function.[3] Velocities (or time-dependent dipoles) are obtained from molecular dynamics run and used as inputs to get the classical spectra.[4] On this regard, our group has recently developed a free-to-use web-platform to allow the user to exploit a time-average technique to get fast and better resolved spectra.[5] This type of classical calculation can be improved with techniques like adiabatic switching (AS)[6–11] or quasi-classical trajectory (QCT) dynamics,[12–16] but it is missing nuclear quantum effects (NQE) once the classical propagation has been performed.

A proper description of IR spectroscopy requires a quantum mechanical treatment. A rough estimate is obtained by means of the double harmonic approximation, which is available in all commercial software. Several techniques such as generalized second-order vibrational perturbation theory (GVPT2),[17, 18] multi-configuration time dependent Hartree (MCTDH),[19–21] or vibrational self-consistent field (VSCF)[22–28] can be employed for better quantum mechanical IR calculations. All of them are more accurate in estimating frequencies than intensities, a general feature found in any theoretical methodology.

Our focus is on semiclassical initial value representation (SCIVR) dynamics, a theoretical approach derived from Feynman's path integral representation of quantum mechanics upon introduction of a stationary phase approximation.[29–31] In SCIVR spectroscopy classical trajectories are evolved in time and then processed

through the semiclassical propagator.[32] In this way, an accurate approximation to the quantum mechanical survival amplitude of an arbitrary wavepacket is obtained, allowing one to get a reliable power spectrum upon Fourier transform of the calculated survival amplitude.[30, 33–40] Several advances have been performed over the years to make semiclassical calculations of power spectra affordable also for large systems.[41, 42] Here we just recall that the basic time averaged propagator demands for Monte-Carlo convergence of the phase space integration, so its rigorous applicability is limited to model systems and small molecules. Our group has developed techniques like the multiple coherent time averaged semiclassical initial value representation (MC TA-SCIVR),[43–45] which has permitted us to employ ab initio on-the-fly dynamics, the divide-and-conquer time averaged semiclassical initial value representation (DC SCIVR),[46–49] whereby large dimensional systems can be studied, and the adiabatic switching semiclassical initial value representation (AS SCIVR) for more accurate calculations.[50–52] The interested reader can find more details in the relevant literature.[53, 54]

Power spectra are a powerful tool to investigate the spectroscopy of molecular species because they allow one to dig into structural features like hydrogen bond networks or solve open experimental issues by assigning complicated spectra.[55] However, they miss to estimate absorption intensities, which would further help identify vibrational features, be useful for analytical purposes, and give additional structural information.

Efforts to move from a semiclassical power spectrum calculation to a semiclassical IR spectrum calculation were performed in our group by developing an approach able to get semiclassical vibrational wavefunctions starting from a set of power spectrum calculations.[56] The wavefunctions were calculated as a linear combination of harmonic counterparts and then used to get intensities on a state-to-state basis according to the square modulus of the transition dipole.[57, 58] A more effective approach for application to larger molecules was developed by overcoming the state-to-state picture.[59] This goal was obtained starting from the lineshape of a set of power spectra, and dividing the spectrum in energy ranges each referring to one of the modes. IR intensities were eventually obtained by weighing densities of states

according to power-spectrum dependent factors and the square modulus of transition dipole moments.

More recently, we have undertaken a different route to semiclassical IR (SC IR) spectroscopy.[60] We employed the time-average technique to come up with a working formula for IR spectra in the zero-temperature limit, which resembles the time-average formula used for power spectra. The zero-temperature limit provides an excellent approximation to room temperature vibrational spectroscopy for molecules lacking low frequency modes since, under this circumstance, even at room temperature it is the vibrational ground state which is the only state to be sizeably populated. The method, tested on small molecules, is very accurate and able to reproduce selection rules. However, it is based on a double phase-space integration requiring the generation of several thousands of trajectory pairs to reach convergence. This last aspect makes its direct application to larger molecular systems daunting.

In this work we propose a new implementation of the SC-IR method based on the evolution of just a single pair of tailored trajectories per vibrational mode. This new approach, which is inspired by MC TA-SCIVR, is derived upon examination of the application of SC IR to the single harmonic oscillator case. We name the new approach as extended semiclassical IR (e-SC IR). Besides the minimal number of trajectories, e-SC IR features a mode-selective treatment of dipole linearization and an approximation to the real part of the coherent state overlap, which makes application of the method to large molecules doable.

The paper is organized as follows: In the Methodology Section we demonstrate the foundations of our new approach. In the Results and Discussion Section we apply the method to molecules like water, formaldehyde, methane, ethanol, and glycine. Finally, the paper ends with the Conclusions Section.

II. METHODOLOGY

We start off by recalling the basic working formula of SC IR[60]

$$\sigma(\omega,T) = \frac{(2\pi\hbar)^{-2N_\nu}}{2\pi T_s} \iint d\boldsymbol{p}_0 d\boldsymbol{Q}_0 \iint d\boldsymbol{p}'_0 d\boldsymbol{Q}'_0 \times \left| \int_0^{T_s} e^{i\left[S_t(\boldsymbol{p}'_0,\boldsymbol{Q}'_0) - S_t(\boldsymbol{p}_0,\boldsymbol{Q}_0) - \hbar\omega t + \phi'(t) - \phi(t)\right]/\hbar} \langle \boldsymbol{p}_t\boldsymbol{Q}_t|\hat{\mu}\hat{B}(\beta/2)|\boldsymbol{p}'_t\boldsymbol{Q}'_t\rangle \, dt \right|^2 , \tag{1}$$

where $\sigma(\omega,T)$ is the absorption lineshape, N_v is the number of vibrational degrees of freedom, $\boldsymbol{p}_0, \boldsymbol{Q}_0, \boldsymbol{p}'_0, \boldsymbol{Q}'_0$ are the initial phase-space conditions of the trajectory pairs, T_s is the simulation time, $S_t(\boldsymbol{p}_0, \boldsymbol{Q}_0)$ and $S_t(\boldsymbol{p}'_0, \boldsymbol{Q'}_0)$ indicate the instantaneous classical actions, ϕ and ϕ' are the phases of the Herman-Kluk prefactors. Time-evolution of the latter requires the calculation of the Hessian matrix along the trajectories. $\boldsymbol{Q} = \boldsymbol{q} - \boldsymbol{q}_{eq}$ is the normal-mode displacement from equilibrium. The trajectory whose phase space variables are not primed $(\mathbf{p}, \mathbf{Q})$ is excited by means of a harmonic quantum of energy, while the primed phase space variables, i.e. $\mathbf{p}', \mathbf{Q}'$, refer to the trajectory characterized by the zero-point energy. The braket $\langle \boldsymbol{p}_t\boldsymbol{Q}_t|\hat{\mu}\hat{B}(\beta/2)|\boldsymbol{p}'_t\boldsymbol{Q}'_t\rangle$, in which the dipole moment $(\hat{\mu})$ and Boltzmann $(\hat{B})$ operators appear, can be written in the zero temperature limit as[60]

$$\langle \boldsymbol{p}_t\boldsymbol{Q}_t|\hat{\mu}|\Psi_0\rangle \langle \Psi_0|\boldsymbol{p}'_t\boldsymbol{Q}'_t\rangle \approx \left[\sum_{j=1}^{N_\nu} \left.\frac{\partial \boldsymbol{\mu}}{\partial q_j}\right|_{\boldsymbol{q}_{eq}} \left(\frac{Q_t^{(j)}}{2} - \frac{i}{2\omega_j} p_t^{(j)}\right)\right] \langle \boldsymbol{p}_t\boldsymbol{Q}_t|\Psi_0\rangle \langle \Psi_0|\boldsymbol{p}'_t\boldsymbol{Q}'_t\rangle . \tag{2}$$

The overlap between the harmonic ground state and a coherent state can be calculated analytically, since

$$\langle \Psi_0|\boldsymbol{p}_t\boldsymbol{Q}_t\rangle = \prod_{j=1}^{N_\nu} \langle \Psi_0^{(j)}|p_t^{(j)}Q_t^{(j)}\rangle , \tag{3}$$

with[60]

$$\langle \Psi_0^{(j)}|p_t^{(j)}Q_t^{(j)}\rangle = \exp\left\{-\frac{\omega_j}{4\hbar}\left[Q_t^{(j)}\right]^2 - \frac{1}{4\hbar\omega_j}\left[p_t^{(j)}\right]^2 - \frac{i}{2\hbar}p_t^{(j)}Q_t^{(j)}\right\} . \tag{4}$$

We point out that the time-averaged expression in Eq. 1 is not the basic SC formula. As reported in our previous work,[60] a separable approximation to the prefactor and a change in the Fourier integral limits were needed to derive an effective working formula as already shown by Kaledin and Miller in their pioneering work.[41]

A. The harmonic oscillator

We now work out the case of a single harmonic oscillator of frequency ω_0, which can be exactly treated by semiclassical dynamics. The classical mass-scaled Hamiltonian is $H = p^2/2 + \omega_0^2 Q^2/2$. If p_0, Q_0 are the initial conditions, then by solving the classical equations of motion one gets

$$\begin{cases} Q(t) = & Q_0 \cos\omega_0 t + \dfrac{p_0}{\omega_0}\sin\omega_0 t \\ p(t) = & -\omega_0 Q_0 \sin\omega_0 t + p_0 \cos\omega_0 t \end{cases} \tag{5}$$

Based on Eq.5, we break Eq. 1 into several pieces and evaluate each one of them. We start with the Herman-Kluk prefactor $C_t(p_0, q_0)$

$$\begin{aligned} C_t(p_0, Q_0) =& \left[\frac{1}{2}\left(\frac{\partial Q_t}{\partial Q_0} + \frac{\partial p_t}{\partial p_0} - i\omega_0 \frac{\partial Q_t}{\partial p_0} + \frac{i}{\omega_0}\frac{\partial p_t}{\partial Q_0}\right)\right]^{1/2} \\ =& \left[\frac{1}{2}\left(\cos\omega_0 t + \cos\omega_0 t - i\sin\omega_0 t - i\sin\omega_0 t\right)\right]^{1/2} \\ =& e^{-i\omega_0 t/2} \end{aligned} \tag{6}$$

The phase of the prefactor, $\phi_t = -\omega_0 t/2$, is trajectory-independent. Therefore, the term $\phi_t' - \phi_t$ in Eq.1 vanishes for the single harmonic oscillator or for a set of uncoupled harmonic oscillators, and it cannot be responsible for the appearance of the peak at frequency ω_0 expected for the harmonic oscillator under investigation.

We move to the calculation of the classical action along the excited trajectory

$$\begin{aligned} S_t(p_0, Q_0) =& \int_0^t \left(\frac{p_{t''}^2}{2} - \frac{\omega_0^2 Q_{t''}^2}{2}\right) dt'' \\ =& \int_0^t \left(\frac{p_0^2}{2}\cos(2\omega_0 t'') - \frac{\omega_0^2 Q_0^2}{2}\cos(2\omega_0 t'') - \omega_0 p_0 Q_0 \sin(2\omega_0 t'')\right) dt'' \\ =& \frac{p_0 Q_0}{2}(\cos 2\omega_0 t - 1) + \frac{1}{4}\left(\frac{p_0^2}{\omega_0} - \omega_0 Q_0^2\right)\sin(2\omega_0 t). \end{aligned} \tag{7}$$

We evaluate the argument of the complex exponential in Eq.4

$$\frac{1}{2} p_t Q_t = \frac{p_0 Q_0}{2}\cos(2\omega_0 t) + \frac{1}{4}\left(\frac{p_0^2}{\omega_0} - \omega_0 Q_0^2\right)\sin(2\omega_0 t). \tag{8}$$

The results reported in Eq.7 and Eq.8 are similar (they just differ for the $-p_0Q_0/2$ term), and we notice that

$$\exp\left\{\frac{i}{\hbar}\left[S(p_0',Q_0')-S_t(p_0,Q_0)\right]\right\}\exp\left[-\frac{i}{2\hbar}(p_t'Q_t'-p_tQ_t)\right]=\exp\left[\frac{i}{2\hbar}\left(p_0Q_0-p_0'Q_0'\right)\right]. \tag{9}$$

The last complex-valued term that remains to examine is the term appearing in the brackets of Eq.2. Its straightforward evaluation (based on Eq.5) leads to

$$\left.\frac{d\mu}{dq}\right|_{q_{eq}}\left(\frac{Q_t}{2}-\frac{i}{2\omega_0}p_t\right)=\left.\frac{d\mu}{dq}\right|_{q_{eq}}\left(\frac{Q_0}{2}+\frac{p_0}{2i\omega_0}\right)e^{i\omega_0 t}, \tag{10}$$

which means that the time evolution of this term is determined by the phase factor $e^{i\omega_0 t}$. It is this term, combined with the $e^{-i\omega t}$ term related to the Fourier transform, that yields the peak exactly at the ω_0 frequency in the calculated IR spectrum, provided the result in Eq.9 is equal to one and so it is not influential. Therefore, a practical way to perform a single-trajectory-pair simulation, based on Eq.1, which returns the correct frequency value for the harmonic oscillator, is to start both trajectories from the equilibrium geometry, i.e. $Q_0 = Q_0' = 0$. For the sake of completeness, it should be noted that other choices would lead to the annihilation of the exponent in Eq. 9, namely setting $P_0 = P_0' = 0$ or, in general, $P_0Q_0 = P_0'Q_0'$. However, these possibilities are not practical due to the non-separability of the potential ($P_0 = P_0' = 0$), or because they take Eq. 1 towards the classical limit losing quantum effects ($P_0Q_0 = P_0'Q_0'$).

The intensity of the transition is determined by the non-exponential term in Eq.10 and the real-valued exponential in Eq.4. We focus on this last term and notice that

$$\exp\left\{-\frac{\omega_0}{4\hbar}\left[Q_t\right]^2-\frac{1}{4\hbar\omega_0}\left[p_t\right]^2-\frac{\omega_0}{4\hbar}\left[Q_t'\right]^2-\frac{1}{4\hbar\omega_0}\left[p_t'\right]^2\right\}=\exp\left\{-\frac{1}{2\hbar\omega_0}\left(E_t^{harm}+E_t'^{harm}\right)\right\}, \tag{11}$$

which, for the harmonic oscillator, is a constant. According to the harmonic quantization and based on an excitation energy equal to $\hbar\omega_0$, by choosing $E_0^{harm} = 3\hbar\omega_0/2$, and $E_0'^{harm} = \hbar\omega_0/2$ Eq. 11 becomes frequency-independent. Therefore, the following choice of initial conditions for the two trajectories

$$\begin{cases} Q_0 = 0 & p_0 = \sqrt{3\omega_0} \\ Q_0' = 0 & p_0' = \sqrt{\omega_0} \end{cases} \tag{12}$$

is the one which returns the correct harmonic frequency and predicts that the absorption intensity depends on the dipole derivative and the frequency only through Eq.10. The analytical results obtained in this Section are also valid in the case of a set of uncoupled harmonic oscillators.

B. Molecules

Non-linear molecules are made of $3N-6$ (N being the number of atoms in the molecule) anharmonic oscillators coupled to each other. A description based on just a single pair of trajectories is expected to return an approximate estimate of vibrational transition intensities and frequencies. However, the goal to describe at least qualitatively or semi-quantitatively an IR spectrum including quantum effects by employing just a single trajectory pair is important to extend the applicability of quantum (semiclassical) IR calculations to larger and larger molecular systems in a computationally affordable way.

Our starting point is the MC-TA-SCIVR technique developed for power spectra by which accurate frequencies of vibrations can be obtained upon evolution of single tailored trajectories in a mode-by-mode fashion.[44] MC TA-SCIVR adopts harmonic quantization for the initial conditions of the trajectory and a reference wavepacket made of an appropriate combination of coherent states. This choice is made to separate the signal of the investigated mode from all other signals as much as possible. The technique provides exact frequency results when dealing with the single or uncoupled harmonic oscillator, and a very good approximation in other instances.

For calculations of IR spectra, we borrow the recipe of the MC-TA-SCIVR technique, but since no arbitrary wavepacket is present in Eq.1, we have to define a new way to single out the investigated mode. This is done on the basis of the results found in the previous Section and, in particular, we focus on Eq.10. We know that modes that are not IR active are characterized, within the dipole linearization ap-

proximation, by a dipole derivative equal to zero. Therefore, our approach is to set to zero the dipole derivatives of all modes but the i-th mode under investigation (in the following we use label i for the mode to study and label j for all other modes)

$$\frac{\partial \boldsymbol{\mu}}{\partial q_j} = \begin{cases} \dfrac{\partial \boldsymbol{\mu}}{\partial q_i} & \text{if} \quad j = i \\ 0 & \text{if} \quad j \neq i \end{cases} . \tag{13}$$

Eq.2 suggests that a sum over mode contributions has to be taken to get the IR intensities. Ideally, one would like to have no contributions from modes other than the i-th mode to the intensity associated with the fundamental transition involving the i-th mode. So, modes strongly coupled to the i-th mode need to be quenched to avoid spoiling the estimate of the relative transition intensities. We keep the choice of initial conditions for the two trajectories as in Eq.12 for the i-th mode, while we use $p'_0 = p_0 = \sqrt{\omega_j}$ for the other modes. However, we give no initial energy to the lowest-frequency modes since they are usually related to large amplitude motions involving the whole molecule, and no initial energy to modes close in frequency to the i-th mode because they could be dynamically coupled to it.

The intensity of transitions is also determined by the real-valued exponential in Eq.11. In the harmonic oscillator case, this term can be overlooked because we are not interested in the absolute intensity of the IR transition. In the general molecular case we are interested in relative intensities, and we make the approximation to calculate the factors in Eq.11 for the i-th mode only, while we neglect them for the other modes. The rationale for this choice comes not only from the correspondence to the harmonic oscillator case, but also from the observation that in this way we are introducing a new sort of simplified divide-and-conquer technique, which is much less elaborated than the one adopted for power spectra. For a molecule, the real-valued exponential in the l.h.s. of Eq. 11 decays in time because the trajectory is not returning periodically to the equilibrium geometry, but it is often diverting to other regions of the phase space. This phenomenon is statistically more and more probable for larger and larger molecular systems. By limiting the real-valued exponential to one mode at a time, we overcome the curse of dimensionality issue.

As for the vibrational frequencies, they are estimated by means of the complex exponentials appearing in Eq.1. In the limit of large simulation times compared

to the timescale of vibrations, each term appearing in the complex exponentiations provides a shift of the calculated frequency. While in the harmonic oscillator case the harmonic ω_0 frequency is returned by the calculation, in the molecular case deviations from the harmonic estimates are found. They are due to the topological anharmonicity of the potential energy surface (PES) and quantum effects. They are accounted for through the $\phi'_t - \phi_t$ difference (which is in general different from zero for molecules) and through the fact that the complex action exponential and the $p_t Q_t$ terms do not compensate exactly anymore even if we start the two trajectories from the equilibrium molecular geometry. For this reason, we calculate the complex exponentials for all modes. We notice that this does not constitute an issue for large dimensional systems since complex exponentials are bounded in magnitude and cannot decay to zero.

The procedure we have illustrated is employed to calculate the absorption lineshape of all molecules we investigate. From there, reminding the reader that we work in the zero-temperature limit, it is easy to get the absorption (IR) spectrum as

$$\alpha(\omega, T \to 0) = \omega\, \sigma(\omega, T \to 0). \tag{14}$$

The relative values of $\alpha(\omega, T \to 0)$ is what we plot in the results presented in the next Section.

III. RESULTS AND DISCUSSION

We apply our e-SC-IR method to a set of molecules of increasing complexity. When available we compare our results with quantum mechanical exact ones or experiments. In some cases the reference is given by SC-IR calculations based on converged integrations. All calculations are performed on analytical PESs starting from the initial conditions illustrated in the previous Section. In all the simulations we present, the two trajectories needed by each mode simulation are evolved with time steps of 10 a.u. for a total of 2500 steps (about 0.6 ps). This simulation time is sufficiently long to allow for several vibrational periods of the molecule. For the propagation of all the trajectories, a fourth-order symplectic integrator is employed.[61] Dipole derivatives at the equilibrium geometry for molecules other

than water have been calculated ab initio by means of the NWChem software,[62] the same way as we did in Ref.60.

A. Water

Figure 1 shows a comparison of the e-SC IR results for the non-rotating water molecule to SC IR results (taken from Ref.60), the double harmonic approximation, and discrete value representation (DVR) results, the latter being considered exact quantum mechanical calculations. The employed PES is the one by Thiel et al.[63] and the dipole derivatives are calculated using the dipole surface by Tennyson et al.[64] In each e-SC-IR simulation focused on one of the stretches the other stretching mode is initially given zero energy. e-SC IR is shown not only to outperform the double harmonic approximation estimates, but also to reproduce reliably all main features, including the frequency anharmonicity, the relative order of intensities, and the presence of overtones and combination bands. Stretch intensities are slightly overestimated and the symmetric stretch frequency is slightly red shifted, but deviations from the exact results are expected since the simulation is based on a single pair of trajectories. However, this peculiar characteristic of e-SC IR allows one to better resolve the individual peaks. This is evident looking at the two stretches, which are resolved in the e-SC-IR calculation, while they show up as a single band in the SC-IR simulation. Furthermore, the intensity of the bending overtone is now more realistically estimated. The increased resolution is the effect of employing as single pair of targeted trajectories (in the case of e-SC IR) instead of a large set of pairs of trajectories initiated from a distribution of initial conditions (in the case of SC IR). Since each pair of trajectories provides a slightly different estimate of frequencies and intensities, it is evident that SC IR is characterized by wider peaks as the result of the sum of the spectral contributions of the different pairs of trajectories employed.

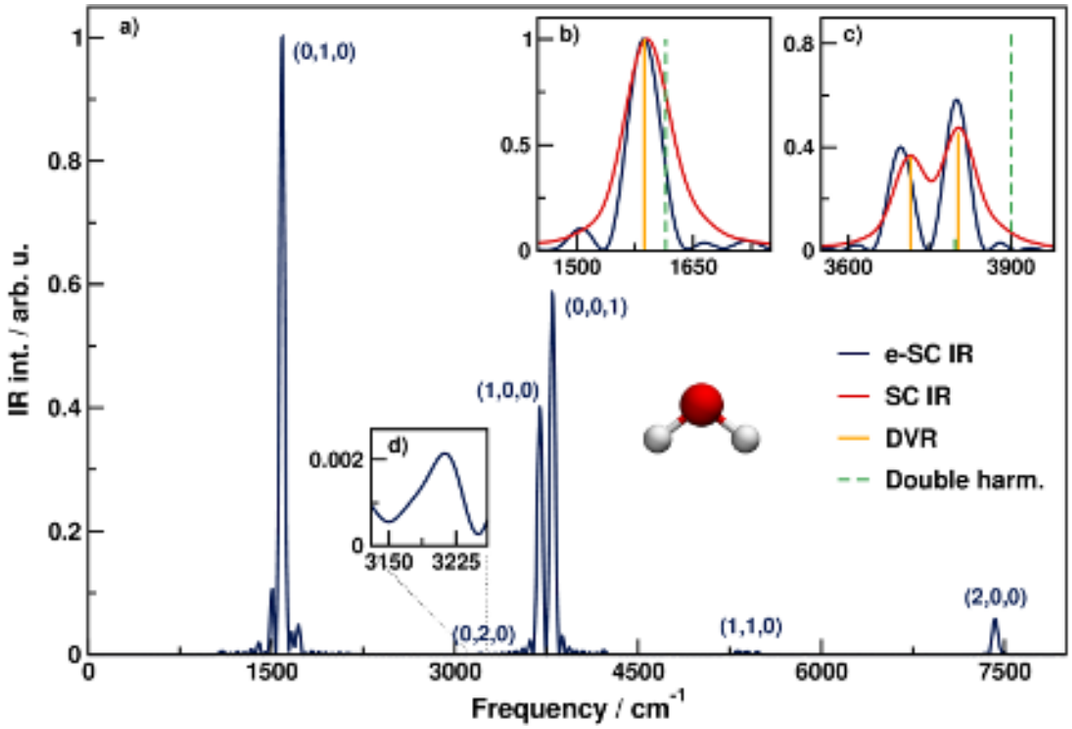

Figure 1: (a) e-SC-IR spectrum of the non-rotating water molecule. The bending and stretch signals are compared to the SC-IR spectrum (red), quantum mechanical DVR results (orange), and double harmonic estimates (dashed green lines) in insets (b) and (c), respectively. Inset (d): Bending overtone.

Table I reports the frequency and intensity values found with different methods including DVR from a previous work[56] (for DVR the intensity of the bending overtone is not available). As expected, e-SC IR provides a less accurate approximation than SC-IR results but the main features of the spectrum are reliably reproduced.

Table I: IR absorption frequencies (cm^{-1}) and relative intensities (arb. units) of the non-rotating water molecule. Triplets (ν_s, ν_b, ν_a) indicate the quanta of excitation of symmetric stretch, bending, and asymmetric stretch, respectively.

	DVR		SC IR		e-SC IR	
Mode	ω	I	ω	I	ω	I
(0,1,0)	1587	1	1591	1	1587	1
(1,0,0)	3715	0.363	3715	0.367	3697	0.400
(0,0,1)	3803	0.456	3804	0.475	3800	0.584
(0,2,0)	3138	-	3166	0.006	3213	0.002

B. Formaldehyde

The study of formaldehyde is undertaken in a similar way to that of water. We employ a pre-existing analytical PES by Martin *et al.*[65] and generate the SC-IR spectrum by means of 100,000 pairs of trajectories. We set a threshold of 10^{-4} on the monodromy matrix determinant, so trajectories for which the monodromy matrix determinant differs from 1 more than 10^{-4} are discarded. In this way we find that 89% of the trajectories must be discarded and do not contribute to the SC-IR spectrum. For the e-SC-IR simulation, we set the initial energy of one of the two CH stretches to zero when the other is under investigation. The two CH stretches of formaldehyde are labeled as mode 5 and mode 6.

In Figure 2 some general features of the e-SC-IR method already present for water are found for formaldehyde too: The agreement between e-SC-IR spectra and SC-IR ones in both frequencies and intensities is pretty good, and e-SC IR is able to provide a better resolved spectrum, which is especially evident in the case of mode 5 and mode 6.

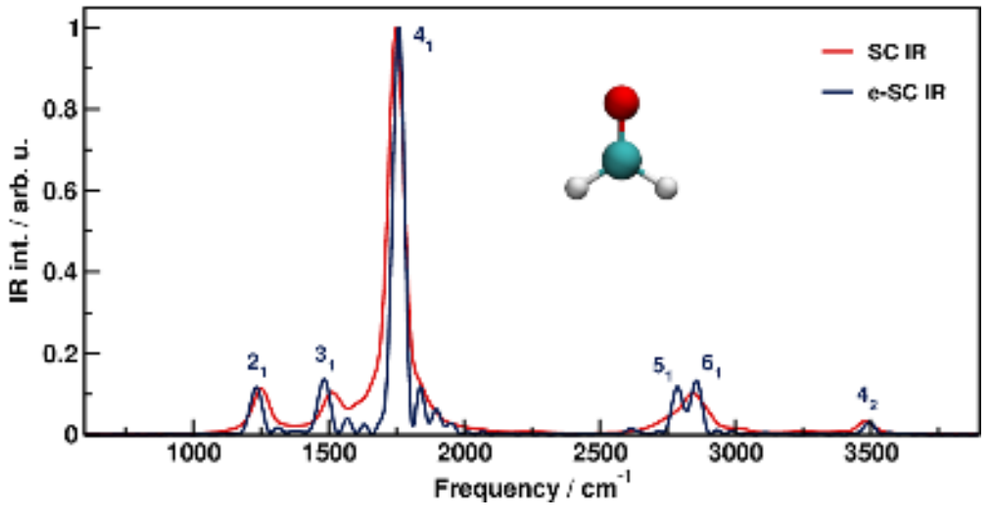

Figure 2: IR spectrum of the non-rotating formaldehyde molecule. e-SC IR (blue) is compared to the SC-IR spectrum (red).

Table II reports vibrational frequencies and intensities for formaldehyde. All modes of formaldehyde are IR active, but mode 1 has a very weak intensity as pointed out by the e-SC-IR calculation. Frequencies obtained with the e-SC-IR calculations are close to the QM ones and intensities reproduce the SC-IR results with good accuracy. Once more, we do notice that by means of e-SC IR we are able to resolve the two CH stretches, and their frequencies are in very good agreement with the reference DVR results.

Table II: IR absorption frequencies (cm^{-1}) and relative intensities (arb. units) of the non-rotating formaldehyde molecule. QM values are taken from Ref. 66. The subscript in the mode number indicates the quanta of excitation.

	QM	SC IR		e-SC IR	
Transition	ω	ω	I	ω	I
1_1	1171	-	-	1149	$\approx 10^{-5}$
2_1	1253	1252	0.113	1233	0.117
3_1	1509	1513	0.104	1484	0.136
4_1	1750	1749	1	1759	1
5_1	2783	-	-	2787	0.118
6_1	2842	2843	0.101	2857	0.133
4_2	3480	3479	0.033	3495	0.031

C. Methane

We keep increasing the complexity of the molecular system to investigate, and move to study the IR spectrum of methane. Methane is characterized by some IR inactive modes but also by triply degenerate modes. The pre-existing PES we employ is the one by Lee *et al.*[67] In a previous paper,[68] we reported SC-IR calculations on the same PES based on 500,000 pairs of trajectories, about 92% of which were rejected according to a monodromy matrix determinant threshold of 10^{-4}. Those SC-IR results are used here for comparison. In our e-SC-IR calculations, which are reported in Figure 3, the modes that are degenerate to the one under investigation are given zero initial energy. Once more, there is very good accuracy in frequencies between the SC-IR spectrum and the e-SC-IR one. The e-SC-IR approach somewhat underestimates the intensity of the first fundamental transition, but general features are maintained at a much lower computational cost. Furthermore, e-SC IR has the nice feature of providing narrower signals.

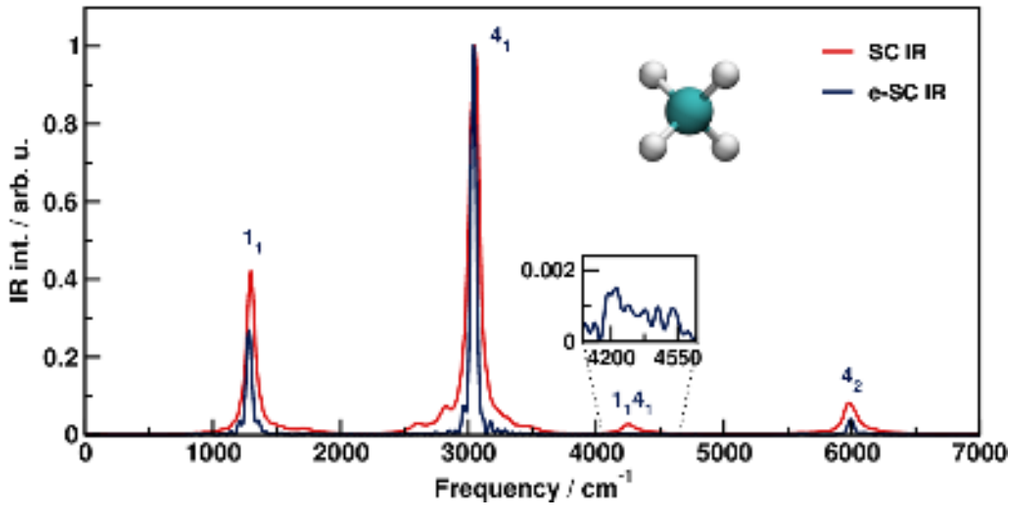

Figure 3: IR spectrum of the non-rotating methane molecule. e-SC IR (blue) is compared to the SC-IR spectrum (red).

Table III gives a detailed overview of the results for the methane molecule. We notice the presence of a combination band above 4000 cm^{-1}: Its intensity is one order of magnitude higher for SC IR than for e-SC IR, as shown in the inset of Figure 3.

Table III: IR absorption frequencies (cm^{-1}) and relative intensities (arb. units) of the non-rotating methane molecule. QM results are taken from Ref. 69, and SC-IR results from Ref. 68. The subscript in the mode number(s) indicates the quanta of excitation.

	QM	SC IR		e-SC IR	
Transition	ω	ω	I	ω	I
1_1	1313	1296	0.420	1283	0.268
2_1	1534	*IR inactive*			
3_1	2949	*IR inactive*			
4_1	3053	3049	1	3040	1
$1_1\,4_1$	-	4252	0.027	4226	0.002
4_2	-	5977	0.081	5992	0.040

D. *Trans*-Ethanol

Trans-ethanol is the global minimum of the ethanol molecule and it is characterized by 21 vibrational degrees of freedom. In our calculations we employ a PES at CCSD(T)-F12a/aug-cc-pVDZ level of theory and built by Nandi et al.[70] already adopted for semiclassical and VSCF power spectrum calculations.[28] In particular, the semiclassical power spectrum was able to correctly detect the Fermi resonance between the CH_2 symmetric stretch and the overtone of the CH_2 wagging.

Figure 4 demonstrates the ability of our extended SC-IR technique to describe with good accuracy the spectral features of ethanol over a large range of frequencies. For the calculations, we give initial zero energy to the first two lowest-frequency modes, which have harmonic estimates under 300 cm^{-1}, and to the modes closest in frequency to the one under consideration, most likely coupled to it. For the fingerprint region, we sorted modes 4-5, 6-8, 9-10, and 11-15 into distinct groups of dynamically coupled modes, while for the higher-frequency region, we divided the CH_2 stretches (modes 16-17) from the CH_3 stretches (modes 18-20).

We stress that the comparison to the reported IR experiment is not intended to be strictly quantitative (at least when looking at intensities) because the experiment we have available also includes rotational features. Intensities (even if not directly comparable) are anyway in reasonable agreement with the experiment. The three main bands making up the IR spectrum of *trans*-ethanol are correctly reproduced. We notice that the lowest-frequency band presents more distinct features compared to the wider-peaked IR ro-vibrational spectrum. Combination bands and overtones are present close to 2000 cm^{-1}, and the anticipated Fermi resonance is clearly visible, with the overtone of the CH_2 wagging responsible for the first peak of the CH band at around 2800 cm^{-1} and the CH_2 symmetric stretch associated to the second peak of the CH band at 2881 cm^{-1}. Finally, the OH stretch is well isolated and its intensity is presumably overestimated, but not exaggeratedly, by our single-pair-trajectory calculation. Overall, our e-SC-IR spectrum appears to be much closer to the experimental results than the IR spectrum obtained through a recent machine-learning-based study.[71] In that study the same experimental reference was adopted.

Table IV points out the general good agreement between the e-SC-IR frequency

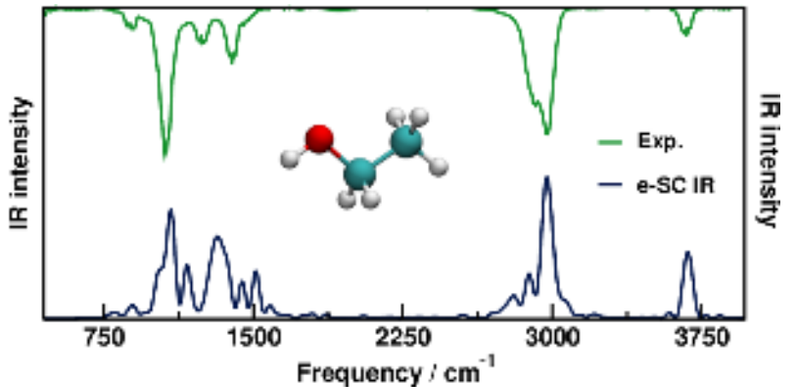

Figure 4: IR spectrum of the non-rotating *trans*-ethanol molecule. Experimental ro-vibrational spectrum (green) and e-SC-IR spectrum (blue).

estimates and those obtained from the experiment and a previous adiabatically switched semiclassical initial value representation (AS SCIVR) calculation. We obtained mode frequencies and intensities by looking at the specific single-mode simulations, i.e. before summing all individual spectra to get the final e-SC-IR spectrum shown in Figure 4. This is what we mean by "single-mode estimate" in Table IV. Single-mode spectra are reported for all molecules in the Supplementary Material file. There are four instances of spectral features that appear split. While the 2803/2881 cm^{-1} pair clearly identifies the already discussed Fermi resonance, the other three cases are due to the decoupling of the low-frequency, large-amplitude modes introduced by our initial zero-energy conditions. This choice is made to better represent high frequency features, and it is successful in this goal, but it may influence the fingerprint region of the IR spectrum. However, the two estimated frequencies for the three just mentioned cases, as reported in Table IV, are in the ball-park of the experimental and AS-SCIVR values and in-between the two e-SC-IR values. Finally, we notice an exchange in the sorting of spectral signals within the CH-stretch band involving mode 17 and mode 18. This may happen due to dynamical effects, especially when the calculation is based on a few trajectories.

Table IV: IR absorption frequencies (cm^{-1}) and relative intensities (arb. units) of the non-rotating *trans*-ethanol molecule. Experimental results are taken from Ref.72. Results labeled as AS SCIVR are found in Ref.28.

	Exp.	AS SCIVR	e-SC IR	
Mode	ω	ω	ω^*	I^*
4	801	-	803	0.051
5	892	-	887	0.085
6	1027	-	1033	0.492
7	1090	1088	1087	1
8	1166	1148	1169	0.431
9	1241	1242	1263	0.046
10	1275	1271	1257	0.011
11	1367	1363	1384	0.001
12	1450	1420	1317/1444	0.817/0.344
13	1455	1440	1422/1498	0.007/0.007
14	1480	1456	1425	0.049
15	1500	1481	1469/1540	0.003/0.001
16	2888	2881	2803/2881**	0.215/0.130
17	2901	2888	2962	0.790
18	2922	2933	2870	0.192
19	2987	2983	2979	0.102
20	2992	2986	2990	0.617
21	3676	3676	3680	0.683

* Single-mode estimate

** Fermi resonance

E. Glycine I

The last molecular system we investigate is glycine in its more stable conformer, known as Conformer I. This system has attracted interest for both its spectroscopic and kinetic features.[27, 73–76] Here we focus on the high-frequency region of the IR spectrum, the one made of the two CH-stretches, the two NH-stretches, and the OH stretch. Glycine is a quite floppy molecule with several conformers separated by small barriers.[77–79] One experimental IR spectrum of isolated glycine at very low temperature is available,[80] and two of us were already involved in the determination of the IR spectrum of glycine by means of a previously developed and elaborated method based on the calculation of semiclassical power spectra.[59]

The experimental spectrum presents a sharp OH-stretch peak and broader and much less intense features for the CH- and NH-stretches. Around 3200 cm^{-1}, it also shows a peak which has been assigned to the OH-stretch of Glycine Conformer II.[80] For the e-SC-IR calculation, we employ a pre-existing PES by Conte et al.[79] at DFT/B3LYP/aug-cc-pVDZ level of theory and give initial zero energy to the three lowest-frequency modes of glycine. Additionally, when we deal with one of the CH stretches, we give no initial energy to the other one. The same applies to the NH stretches. We report the e-SC-IR spectrum in Fig.5. We notice that the OH stretch signal is red-shifted by about 40 cm^{-1} compared to the experiment and broadened due to the contribution of the neighboring NH stretches. The red shift is related to the quenching of the low-frequency modes, which is anyway necessary, according to our method, for a sensible computation of intensities. The CH band covers the same frequency range as the experimental signal, with the two separate stretches clearly visible in our calculation. Furthermore, at around 3200 cm^{-1}, an absorption signal is present and it comes uniquely from our OH-stretch calculation. A possible explanation is that during the dynamics there is a partial interconversion to Conformer II (the energy of the trajectories is much above the interconversion barrier), and this is revealed in the calculated IR spectrum when considering the dynamics of the OH-stretch mode. The e-SC-IR spectrum is calculated based on the differences originated by two trajectories, and this feature allows the calculation to point out conformational differences experienced during the dynamics better than

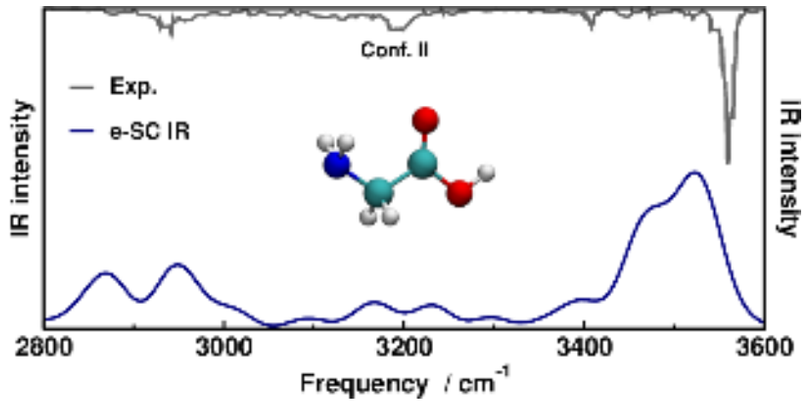

Figure 5: IR spectrum of the non-rotating glycine I molecule. Experimental IR spectrum (gray) and e-SC-IR spectrum (blue). OH-stretch intensities of the experimental and e-SC-IR spectra are matched.

in the case of a power spectrum obtained from a single trajectory, which, due to the short trajectory time (about 0.6 ps), is given not enough time to visit Conformer II.

Table V reports experimental data and the corresponding frequencies and intensities estimated by means of three different theoretical approaches, i.e., the previous semiclassical approach based on MC-TA SCIVR, the generalized second-order perturbation theory method (GVPT2), and our e-SC-IR approach. First of all, we notice that, apart from the case of the OH stretch, it is not easy to determine a precise frequency and intensity for the experimental spectrum, probably due to the presence of a residual small amount of rotational energy in spite of the low temperature at which the spectrum has been recorded. Therefore, in the case of the CH-stretches, we have chosen to provide an estimate of the range of experimental frequencies in which the two CH stretches are found. We notice that one advantage of our e-SC-IR method is that single modes are better resolved, and this is true also compared to the previous MC-TA-SCIVR-based calculation. Frequencies of CH stretches and NH stretches are in very good agreement with the experiment, and their intensities are reasonable too. For the experimental spectral feature at about 3200 cm^{-1}, assigned to glycine Conformer II, we report that our e-SC-IR dynamics-based frequency estimate is much closer than the VPT2 one to the experiment.

Table V: IR absorption frequencies (cm^{-1}) and relative intensities (arb. units) of the non-rotating glycine I molecule. The absorption intensity of the OH stretch is set to 0.25 (the experimental value) for all approaches reported. The e-SC-IR signal matching Conf II is obtained from dynamics started from Conf I. Experimental results are taken from Ref. 80, and GVPT2 from Ref. 74.

	Exp.		Ref. 59		GVPT2		e-SC IR	
Mode	ω	I	ω	I	ω	I	$\omega_{sing}/\omega_{sum}$	I^*
20	2880-2935	0.04	2900	0.07	2938	0.09	2938/2949	0.06
21	2880-2935	0.04	2900	0.07	2929	0.04	2871/2869	0.09
22	3410	0.03	3345	0.03	3387	0.01	3357/3398	0.08
23	3450	0.01	3430	0.01	3407	0.02	3459/3480	0.005
24	3560	0.25	3563	0.25	3568	0.25	3519/3523	0.25
Conf II	3180-3200	0.04	-	-	3235	0.10**	3166-3230	0.04

* Single-mode estimate

** Estimated from Fig. 3 of Ref. 74

IV. SUMMARY AND CONCLUSIONS

We have presented the e-SC-IR technique based on the semiclassical evolution of just one pair of trajectories per vibrational mode under investigation. The approach has been shown to reproduce faithfully the IR spectral features of small and larger size molecules. The latter were not treatable by means of the recently developed time averaged SC-IR technique. e-SC IR is a development of SC IR characterized by the possibility to deal with larger sized molecular systems. This descends not only from the fact that simulations are based on a single pair of trajectories per mode, but also from the peculiar treatment of the overlap involving coherent states, which has been derived from the exact harmonic oscillator case. Rather complicated features like combination bands, overtones, and Fermi resonances are well described with some deviations from benchmark values, which are acceptable due to the gained computational affordability of the approach: In principle, vibrational modes of any system, including solvated ones, are obtainable at the cost of two semiclassical trajectories per mode.

We remark some improvements provided by our e-SC-IR calculations compared to results obtained by means of other techniques. For instance, a recent machine-

learning-based calculation for the IR spectrum of *trans*-ethanol has appeared in the literature,[71] providing a less accurate IR spectrum than ours, especially when looking at absorption intensities. In the case of glycine we were able to resolve the two CH stretches, and to point out a signal assigned to a different conformer by exploiting the dynamics underlying our approach and the possibility to sample geometries distorted compared to the initial equilibrium one, including other conformers. Our e-SC-IR method has been worked out in the zero-temperature limit. While future research will also be devoted to including finite-temperature effects, we remind the reader that even at room temperature most of the population is in the ground vibrational state, especially in the case of molecules lacking very low frequency modes. Finally, we stress that our lineshape is directly obtained from the dynamics without using any *ad hoc* Laurentzian artifact. Therefore, it is remarkable that the general shape of complex bands is reproduced reasonably well by our e-SC-IR method. When dealing with large dimensional systems, sometimes it could be difficult to distinguish between real spectral signals and "aliases", which are due to the discrete sampling of the dynamics. A way to overcome this issue is to employ the Pad\'{e} approach to Fourier transform, so the time-dependent function to be Fourier transformed is represented continously and the "aliases" are no longer found.

Further future developments will concern the application of the method to *ab initio* on-the-fly molecular dynamics and the investigation of some possible technical improvements to increase the accuracy of the approach. For instance, we will investigate the possibility to keep the real exponentiation of Eq. 11 time-independent, but with inclusion of a dependence on the harmonic frequencies of the modes not being investigated. This can be achieved by the calculation of an average harmonic energy along the trajectory. Another possible improvement concerns Eqs. 3 and 4, since they could be evaluated by substituting the single ground-state harmonic wavefunction with a semiclassical wavefunction expanded onto a basis of harmonic vibrational functions. Finally, the initial conditions for the pair of trajectories could be obtained by means of an adiabatic switching technique, similarly to what is done in the AS-SCIVR technique for power spectra, which should warrant better accuracy and precision (i.e. narrower spectral features). Overall, our future work will

be aimed at employing this new technique to calculate the IR spectra of large dimensional systems, which are usually not treatable by other quantum mechanical approaches.

Supplementary Material

Single-mode spectra for all molecules investigated are reported in the Supplementary Material file.

Acknowledgments

C.L. and M.C. acknowledge the European Research Council under Grant Agreement No.101081361—SEMISOFT—ERC-2022-POC2 for funding.

Author Declarations

Conflict of interest

The authors have no conflicts to disclose.

Author Contributions

Cecilia Lanzi: Investigation (equal); Methodology (equal); Software (equal); Validation (equal); Writing – original draft (equal). **Chiara Aieta**: Conceptualization (equal); Methodology (equal); Writing – original draft (equal). **Michele Ceotto**: Conceptualization (equal); Funding acquisition (equal); Methodology (equal); Supervision (equal); Writing – original draft (equal). **Riccardo Conte**: Conceptualization (equal); Funding acquisition (equal); Methodology (equal); Supervision (equal); Writing – original draft (equal).

Data Availability

The data that support the findings of this study are available from the corresponding author upon reasonable request.

Bibliography

[1] J. Haas and B. Mizaikoff, Annu. Rev. Anal. Chem. **9**, 45 (2016).

[2] R. Conte, M. Gandolfi, D. Moscato, C. Aieta, S. Valtolina, and M. Ceotto, J. Comput. Chem. **46**, e70118 (2025).

[3] R. Conte, C. Aieta, G. Botti, M. Cazzaniga, M. Gandolfi, C. Lanzi, G. Mandelli, D. Moscato, and M. Ceotto, Th. Chem. Acc. **142**, 53 (2023).

[4] D. Frenkel and B. Smit, *Molecular simulation: from algorithms to applications* (2000).

[5] M. Gandolfi, D. Moscato, C. Aieta, M. Pindaro, E. Campana, S. Valtolina, and M. Ceotto, *A web platform for time averaged fourier transform of autocorrelated data* (2024), accessed on May 1, 2025, URL `http://semisoft.unimi.it/`.

[6] R. T. Skodje, F. Borondo, and W. P. Reinhardt, J. Chem. Phys. **82**, 4611 (1985).

[7] S. Saini, J. Zakrzewski, and H. S. Taylor, Phys. Rev. A **38**, 3900 (1988).

[8] Q. Sun, J. M. Bowman, and B. Gazdy, J. Chem. Phys. **89**, 3124 (1988).

[9] A. Bose and N. Makri, J. Chem. Phys. **143**, 114114 (2015).

[10] C. Qu and J. M. Bowman, J. Phys. Chem. A **120**, 4988 (2016).

[11] T. Nagy and G. Lendvay, J. Phys. Chem. Lett. **8**, 4621 (2017).

[12] C. Qu and J. M. Bowman, J. Phys. Chem. Lett. **9**, 2604 (2018).

[13] M. Stei, E. Carrascosa, A. Dorfler, J. Meyer, B. Olasz, G. Czako, A. Li, H. Guo, and R. Wester, Sci. Adv. **4**, eaas9544 (2018).

[14] G. Amati, M. A. C. Saller, A. Kelly, and J. O. Richardson, J. Chem. Phys. **157**, 234103 (2022).

[15] D. Barbiero, G. Bertaina, M. Ceotto, and R. Conte, J. Phys. Chem. A **127**, 6213 (2023).

[16] T. L. Fischer, M. Bödecker, S. M. Schweer, J. Dupont, V. Lepère, A. Zehnacker-Rentien, M. A. Suhm, B. Schröder, T. Henkes, D. M. Andrada, et al., Phys. Chem.

Chem. Phys. **25**, 22089 (2023).

[17] V. Barone, M. Biczysko, and J. Bloino, Phys. Chem. Chem. Phys. **16**, 1759 (2014).

[18] Q. Yang and J. Bloino, J. Phys. Chem. A **126**, 9276 (2022).

[19] H.-D. Meyer, U. Manthe, and L. S. Cederbaum, Chem. Phys. Lett. **165**, 73 (1990).

[20] U. Manthe, J. Chem. Phys. **128**, 164116 (2008).

[21] D. Picconi, J. A. Cina, and I. Burghardt, J. Chem. Phys. **150**, 064112 (2019).

[22] J. M. Bowman, S. Carter, and X. Huang, Int. Rev. Phys. Chem. **22**, 533 (2003).

[23] Y. Wang, S. Carter, B. J. Braams, and J. M. Bowman, **128**, 071101 (2008).

[24] K. Yagi, M. Keceli, and S. Hirata, J. Chem. Phys. **137**, 204118 (2012).

[25] B. Thomsen, K. Yagi, and O. Christiansen, J. Chem. Phys. **140**, 154102 (2014).

[26] Q. Yu and J. M. Bowman, J. Chem. Phys. **146**, 121102 (2017).

[27] C. Qu, P. L. Houston, R. Conte, A. Nandi, and J. M. Bowman, J. Phys. Chem. A **125**, 5346 (2021).

[28] R. Conte, A. Nandi, C. Qu, Q. Yu, P. L. Houston, and J. M. Bowman, J. Phys. Chem. A **126**, 7709 (2022).

[29] W. H. Miller, J. Chem. Phys. **53**, 3578 (1970), URL `http://scitation.aip.org/content/aip/journal/jcp/53/9/10.1063/1.1674535`.

[30] W. H. Miller, J. Phys. Chem. A **105**, 2942 (2001).

[31] W. H. Miller, Proc. Natl. Acad. Sci. USA **102**, 6660 (2005).

[32] E. J. Heller, Acc. Chem. Res. **14**, 368 (1981).

[33] K. G. Kay, J. Chem. Phys. **100**, 4377 (1994).

[34] F. Grossmann, Comments At. Mol. Phys. **34**, 141 (1999).

[35] E. Pollak and E. Martin-Fierro, J. Chem. Phys. **126**, 164107 (2007).

[36] M. Wehrle, M. Sulc, and J. Vanicek, J. Chem. Phys. **140**, 244114 (2014).

[37] M. S. Church, T. J. H. Hele, G. S. Ezra, and N. Ananth, J. Chem. Phys. **148**, 102326 (2018).

[38] L. Bonnet, J. Chem. Phys. **153**, 174102 (2020).

[39] T. Begušić and J. Vaníček, J. Chem. Phys. **153**, 024105 (2020).

[40] C. A. Myers, K. Miyazaki, T. Trepl, C. M. Isborn, and N. Ananth, J. Chem. Phys. **161**, 084114 (2024).

[41] A. L. Kaledin and W. H. Miller, J. Chem. Phys. **118**, 7174 (2003).

[42] A. L. Kaledin and W. H. Miller, J. Chem. Phys. **119**, 3078 (2003).

[43] M. Ceotto, S. Atahan, S. Shim, G. F. Tantardini, and A. Aspuru-Guzik, Phys. Chem. Chem. Phys. **11**, 3861 (2009).

[44] M. Ceotto, S. Atahan, G. F. Tantardini, and A. Aspuru-Guzik, J. Chem. Phys. **130**, 234113 (2009).

[45] M. Ceotto, D. Dell' Angelo, and G. F. Tantardini, J. Chem. Phys. **133**, 054701 (2010).

[46] M. Ceotto, G. Di Liberto, and R. Conte, Phys. Rev. Lett. **119**, 010401 (2017).

[47] G. Di Liberto, R. Conte, and M. Ceotto, J. Chem. Phys. **148**, 104302 (2018).

[48] M. Gandolfi, A. Rognoni, C. Aieta, R. Conte, and M. Ceotto, J. Chem. Phys. **153**, 204104 (2020).

[49] A. Rognoni, R. Conte, and M. Ceotto, Chem. Sci. **12**, 2060 (2021).

[50] R. Conte, L. Parma, C. Aieta, A. Rognoni, and M. Ceotto, J. Chem. Phys. **151**, 214107 (2019).

[51] G. Botti, M. Ceotto, and R. Conte, J. Chem. Phys. **155**, 234102 (2021), ISSN 10897690.

[52] G. Botti, C. Aieta, and R. Conte, J. Chem. Phys. **156**, 164303 (2022).

[53] R. Conte, C. Aieta, M. Cazzaniga, and M. Ceotto, J. Phys. Chem. Lett. **15**, 7566 (2024).

[54] R. Conte, G. Mandelli, G. Botti, D. Moscato, C. Lanzi, M. Cazzaniga, C. Aieta, and M. Ceotto, Chem. Sci. **16**, 20 (2025).

[55] F. Gabas, G. Di Liberto, R. Conte, and M. Ceotto, Chem. Sci. **9**, 7894 (2018).

[56] M. Micciarelli, R. Conte, J. Suarez, and M. Ceotto, J. Chem. Phys. **149**, 064115 (2018).

[57] C. Aieta, M. Micciarelli, G. Bertaina, and M. Ceotto, Nat. Comm. **11**, 4384 (2020).

[58] C. Aieta, G. Bertaina, M. Micciarelli, and M. Ceotto, J. Chem. Phys. **153**, 214117 (2020).

[59] M. Micciarelli, F. Gabas, R. Conte, and M. Ceotto, J. Chem. Phys. **150**, 184113 (2019).

[60] C. Lanzi, C. Aieta, M. Ceotto, and R. Conte, J. Chem. Phys. **160**, 214107 (2024).

[61] M. L. Brewer, J. S. Hulme, and D. E. Manolopoulos, J. Chem. Phys. **106**, 4832 (1997).

[62] M. Valiev, E. Bylaska, N. Govind, K. Kowalski, T. Straatsma, H. Van Dam, D. Wang, J. Nieplocha, E. Apra, T. Windus, et al., Comput. Phys. Commun. **181**, 1477 (2010), ISSN 0010-4655, URL https://www.sciencedirect.com/science/article/pii/S0010465510001438.

[63] S. Dressler and W. Thiel, Chem. Phys. Lett. **273**, 71 (1997).

[64] L. Lodi, J. Tennyson, and O. L. Polyansky, J. Chem. Phys. **135**, 034113 (2011).

[65] J. Martin, T. J. Lee, and P. Taylor, J. Mol. Spectr. **160**, 105 (1993).

[66] S. Carter, N. Pinnavaia, and N. C. Handy, Chem. Phys. Lett. **240**, 400 (1995).

[67] T. J. Lee, J. M. Martin, and P. R. Taylor, J. Chem. Phys. **102**, 254 (1995).

[68] C. Aieta, M. Cazzaniga, D. Moscato, C. Lanzi, L. Bocchi, M. M. Costanza, M. Ceotto, and R. Conte, Rend. Lincei Sci. Fis. Nat. pp. 1–11 (2025).

[69] S. Carter, H. M. Shnider, and J. M. Bowman, J. Chem. Phys. **110**, 8417 (1999).

[70] A. Nandi, R. Conte, C. Qu, P. L. Houston, Q. Yu, and J. M. Bowman, J. Chem. Theory and Comput. **18**, 5527 (2022).

[71] Y.-F. Hou, C. Wang, and P. O. Dral, J. Phys. Chem. A **129**, 3613 (2024).

[72] J. R. Durig, H. Deeb, I. D. Darkhalil, J. J. Klaassen, T. K. Gounev, and A. Ganguly, J. Mol. Struct. **985**, 202 (2011).

[73] R. Wu and T. B. McMahon, J. Am. Chem. Soc. **129**, 4864 (2007), ISSN 00027863.

[74] M. Biczysko, J. Bloino, I. Carnimeo, P. Panek, and V. Barone, J. Mol. Struct. **1009**, 74 (2012), ISSN 0022-2860.

[75] V. Barone, M. Biczysko, J. Bloino, and C. Puzzarini, J. Chem. Theory Comput. **9**, 1533 (2013).

[76] G. Mandelli, L. Corneo, and C. Aieta, J. Phys. Chem. Lett. **14**, 9996 (2023).

[77] A. G. Csaszar, J. Am. Chem. Soc. **114**, 9568 (1992).

[78] F. Gabas, R. Conte, and M. Ceotto, J. Chem. Theory Comput. **13**, 2378 (2017), ISSN 15499626.

[79] R. Conte, P. L. Houston, C. Qu, J. Li, and J. M. Bowman, J. Chem. Phys. **153**, 244301 (2020), URL https://doi.org/10.1063/5.0037175.

[80] S. G. Stepanian, I. D. Reva, E. D. Radchenko, M. T. S. Rosado, M. L. T. S. Duarte,

R. Fausto, and L. Adamowicz, J. Phys. Chem. A **102**, 1041 (1998).